LBL-21198
Preprint

Lawrence Berkeley Laboratory
UNIVERSITY OF CALIFORNIA

Physics Division

Submitted to Astrophysical Journal

NEW MEASUREMENTS OF THE COSMIC BACKGROUND RADIATION TEMPERATURE AT 3.3 mm WAVELENGTH

C. Witebsky, G. Smoot, G. De Amici,
and S.D. Friedman

February 1986

Prepared for the U.S. Department of Energy under Contract DE-AC03-76SF00098

NEW MEASUREMENTS OF THE COSMIC BACKGROUND RADIATION TEMPERATURE AT 3.3 mm WAVELENGTH

Chris Witebsky, George Smoot, Giovanni De Amici [1], and Scott D. Friedman [2]

Space Sciences and Lawrence Berkeley Laboratories
University of California, Berkeley

ABSTRACT

We have measured the temperature of the cosmic background radiation (CBR) at 3.3 mm wavelength in 1982, 1983, and 1984 as part of a larger project to determine the CBR temperature at five wavelengths from 12 cm to 3.3 mm (Smoot *et al.* 1985). The 3.3-mm measurements yield a brightness temperature of 2.57 K with a 1σ uncertainty of ± 0.12 K. This paper describes the instrument, the measurement techniques, and the data-analysis procedures used. Our result is in good agreement with recent measurements at comparable wavelengths by Meyer and Jura (1985) and by Peterson, Richards, and Timusk (1985), but it disagrees with the temperatures reported by Woody and Richards (1981).

I. INTRODUCTION

The spectrum of the cosmic background radiation contains a record of interactions between matter and radiation throughout the history of the universe (Peebles 1971; Danese and De Zotti 1977). Any transfer of kinetic or thermal energy from the matter in the universe to the radiation field must alter the spectrum of the radiation from its initial form. After energy transfer the distorted CBR spectrum evolves toward a blackbody distribution, but if the transfer occurs at a redshift smaller than a few times 10^6, there is not enough time to establish a Planck spectrum. Non-radiative Compton scattering and bremsstrahlung, the two main mechanisms for energy transfer, combine to produce a spectrum that is roughly Planckian, but with distortions characteristic of the amount, redshift, and mechanism of energy transfer.

By the late 1970's it was apparent that existing CBR measurements at wavelengths longer than 3 mm did not rule out potentially observable, cosmologically significant distortions. When Danese and De Zotti (1978) fitted model distortions to existing measurements, they found that distortions of up to a kelvin could exist in the Rayleigh-Jeans region without contradicting the available observations. To reduce this uncertainty, we remeasured the CBR Rayleigh-Jeans spectrum in collaboration with research groups headed by G. Sironi of the Istituto Fisica Cosmica, Consiglio Nazionale delle Ricerche (CNR) at Milano, Italy; N. Mandolesi of the Istituto Tecnologia e Studio della Radiazione Extraterrestre, CNR, at Bologna, Italy; R. B. Partridge of Haverford College, Haverford, Pennsylvania; and L. Danese and G. De Zotti of the Universitá di Padova, Italy (Smoot *et al.* 1983, 1985).

The collaborators made measurements at five wavelengths between 12 and 0.33 cm. Milano provided a 12-cm radiometer (Sironi and Bonelli 1986), Bologna supplied a matched 6.3-cm instrument (Mandolesi *et al.* 1986), and Berkeley provided radiometers operating at 3 cm (Friedman *et al.* 1984; Friedman 1984), 9.1 mm (De Amici *et al.* 1985), and 3.3 mm. Berkeley also built a cryogenic reference load used by all five radiometers for absolute calibrations (Smoot *et al.* 1983). Haverford supplied a 3.2-cm radiometer designed as an atmospheric monitor (Partridge *et al.* 1984), and Padova provided theoretical support both in the interpretation of results and in the modeling of atmospheric emission. All six radiometers were used to make measurements

[1]On leave from the Instituto di Radioastronomia CNR, Bologna, Italy.

[2]Now at the University of California, San Diego.

in the summers of 1982 and 1983. The Berkeley group returned again in 1984 for a third set of measurements at 3 cm, 9.1 mm, and 3.3 mm.

This paper reports the results of our measurements at 3.3 mm and describes the instrument and the data-analysis procedures. The measurements from all three years are discussed here, although because of the systematic errors in the 3.3-mm result from 1982 and the statistical uncertainties in the 1984 result, these values are less significant than the one obtained from the 1983 measurements.

II. EXPERIMENTAL CONCEPTS AND REQUIREMENTS

a) Radiometer Concepts

A radiometer measures power per unit bandwidth, typically in units of antenna temperature. The antenna temperature T_A of an isotropic blackbody radiation field with a physical temperature T is given by the equation

$$T_A = \frac{T_\nu}{\exp(T_\nu/T) - 1}\,, \tag{1}$$

where T_ν, defined as

$$T_\nu = h\nu/k\,,$$

characterizes the transition from the Rayleigh-Jeans regime ($h\nu << kT$) to the Wien regime ($h\nu >> kT$). In the Rayleigh-Jeans limit, the antenna temperature of a blackbody is approximately equal to its blackbody temperature. At 3.3-mm wavelength, T_ν has the value 4.32 K.

A Dicke radiometer measures the difference in antenna temperature of the sources at its two input ports. If the ports receive radiation from blackbodies at antenna temperatures $T_{A,1}$ and $T_{A,2}$, the radiometer produces an output voltage of the form

$$V_{\rm out} = \frac{1}{G}[(T_{A,1} - T_{A,2}) + T_{\rm Offset}]\,,$$

where G is the calibration coefficient and $T_{\rm Offset}$ is the instrument-generated offset.

b) Principles of CBR Measurement

To obtain the CBR antenna temperature ($T_{A,\rm CBR}$) one measures the antenna temperature of the zenith ($T_{\rm Zenith}$) and then eliminates the radiative contributions from sources other than the CBR. One performs the measurement by comparing the radiation flux from the zenith with the radiation emitted by a cryogenic reference load at a known antenna temperature, $T_{A,\rm Load}$. The antennas are pointed at the zenith and the cryogenic reference load (or cold load), and the radiometer response voltage, $V_{\rm Zenith/Load}$, is recorded. The radiometer is then rotated so that the targets are exchanged, and the new response voltage, $V_{\rm Load/Zenith}$, is recorded. When the two voltages are differenced, the result is twice the zenith/cold-load voltage with the offset removed. The value of $T_{A,\rm Load}$ is known, so the zenith antenna temperature is given by the formula:

$$T_{\rm Zenith} = \frac{G}{2}(V_{\rm Zenith/Load} - V_{\rm Load/Zenith}) + T_{A,\rm Load}\,.$$

This equation does not include small corrections for instrumental effects, discussed in § VI.

An antenna pointed toward the zenith receives radiation from a variety of sources, local and distant. By far the largest noncosmological component of $T_{\rm Zenith}$ at 3.3 mm is $T_{A,\rm Atm}$, the thermal radiation from water and oxygen molecules in the atmosphere, whose value is roughly equal to the product of the atmosphere's zenith opacity and its average physical temperature. Atmospheric emission at 3.3 mm is substantial and variable: measurements of $T_{A,\rm Atm}$ made in Berkeley on clear nights have yielded values from 25 to 45 K depending upon the atmospheric

water-vapor content. Furthermore, the clumpy nature of the water-vapor distribution can cause the measured temperature to change by several tenths of a kelvin in a matter of minutes. One can reduce $T_{A,\mathrm{Atm}}$ to 10 K or less by observing from a high-altitude, low-humidity site, but this value is still large compared to T_{CBR}.

To remove $T_{A,\mathrm{Atm}}$ from T_{Zenith} requires independent knowledge of $T_{A,\mathrm{Atm}}$, obtained from zenith scans. In the absence of atmospheric self-absorption, the atmospheric component of the sky temperature at a zenith angle Z would be proportional to the air mass, which varies as a known function of Z [approximately as $\sec(Z)$ except near $Z = 90°$]. By measuring the sky temperature at two zenith angles, one can determine its variation with Z and derive a value for $T_{A,\mathrm{Atm}}$. To correct this value for self-absorption, one needs to have additional information about atmospheric properties, either the physical temperature or the opacity. However, this information need not be precise since the correction is small (~300 mK). Temperature profiles derived from standard atmospheric models are adequate.

Other potential noncosmological sources of radiation include the sun ($T_{A,\mathrm{Sun}}$), the moon ($T_{A,\mathrm{Moon}}$), the galaxy ($T_{A,\mathrm{Galaxy}}$), and the ground, both near the radiometer and near the horizon ($T_{\mathrm{Gnd,Zenith}}$). Careful equipment design, choice of observing times, choice of wavelength, and site selection all help to reduce these backgrounds: measurements of T_{CBR} can be made at times when the sun and moon are not observed by the antennas; radiation from the galaxy, a serious source of contamination at longer wavelengths, contributes less than 1 mK to the zenith temperature at 3.3 mm; ground radiation can be reduced to the millikelvin level through the use of low-sidelobe antennas and careful ground shielding. Once the noncosmological contributions have been evaluated, one can calculate the CBR antenna temperature from the formula

$$T_{A,\mathrm{CBR}} = T_{\mathrm{Zenith}} - T_{A,\mathrm{Atm}} - T_{A,\mathrm{Sun}} - T_{A,\mathrm{Moon}} - T_{A,\mathrm{Galaxy}} - T_{\mathrm{Gnd,Zenith}}.$$

The inverse of equation (1) is used to convert this value to the brightness temperature, T_{CBR}.

III. DESCRIPTION OF APPARATUS AND PROCEDURES

a) Observing Site

We observed from the Barcroft Laboratory of the White Mountain Research Station, located near Bishop, California at an altitude of 3800 meters. This facility has been used by a number of researchers for CBR temperature measurements (Ewing *et al.* 1967; Stokes *et al.* 1967; Welch *et al.* 1967; Wilkinson 1967). The site chosen for the observations was a relatively flat stretch of ground with a horizon elevation of 18° or less in all directions. The shared cold load, described in § III*c*, was set in a hole in the ground, suspended below the center section of a 20-meter-long set of tracks running east-west. The radiometers were mounted on carts that could be rolled into position over the cold load.

b) Radiometer Description

Figure 1 shows a block diagram of the superheterodyne Dicke radiometer used for the measurements. Two conical corrugated-horn antennas with 7°.5 half-power beamwidths (Jansen *et al.* 1979) acted as input ports. A Dicke switch, chopping at 100 Hz, alternately connected each antenna to the receiver. Radiation passed from the switch through an isolator and into a double-sideband, balanced mixer whose intermediate frequency band covered the range from 0.1 to 1.0 GHz. A 90-GHz Gunn-effect local oscillator provided the mixer's reference signal. The downconverted signal was amplified by ~60 dB and rectified by a detector diode. The 100-Hz square-wave component in the rectified output voltage had an amplitude proportional to the difference in the antenna temperatures at the two input ports. This signal was processed by a lockin amplifier to produce an output voltage proportional to the difference in the antenna temperatures, averaged over a two-second time interval.

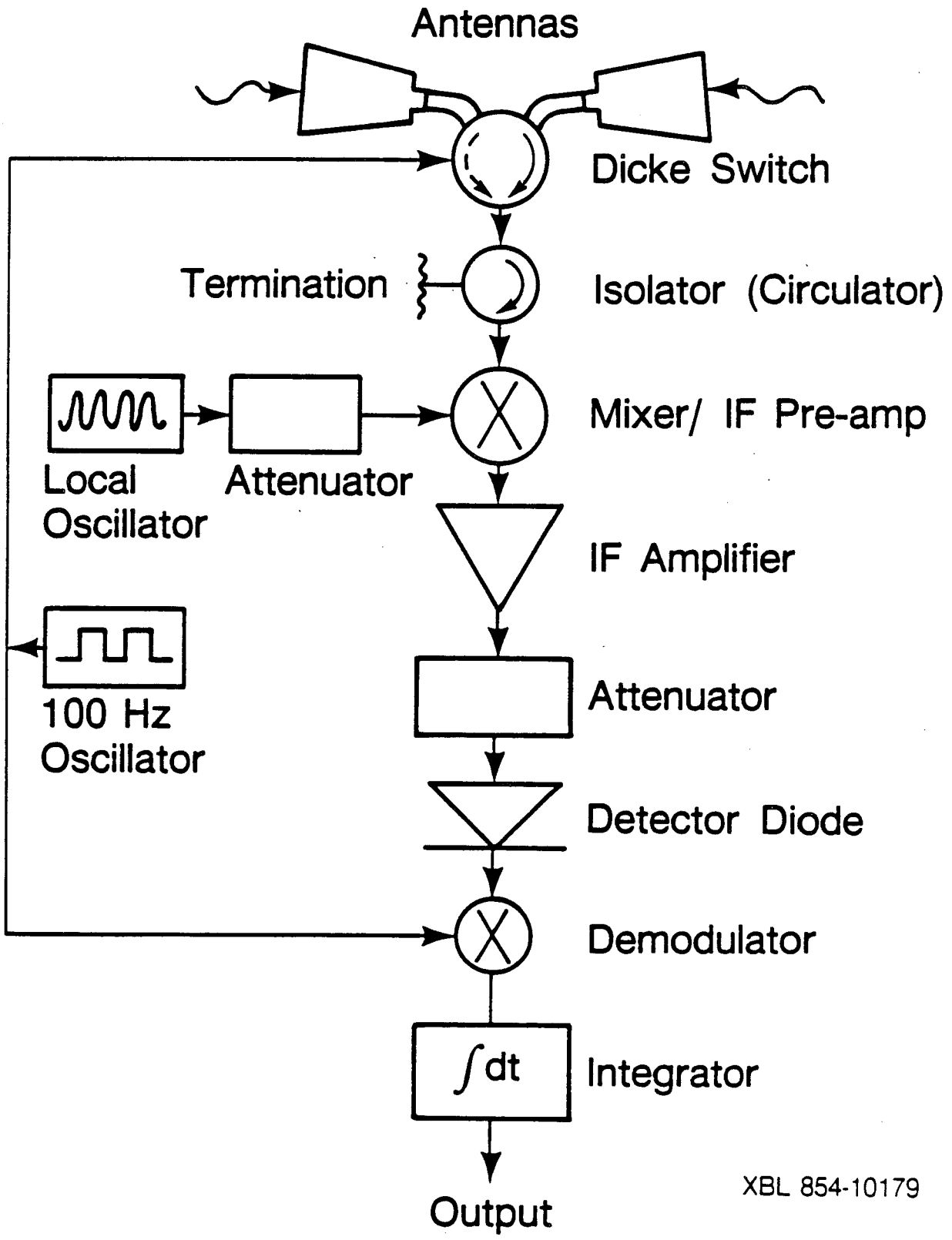

Figure 1: Radiometer block diagram (1982 configuration).

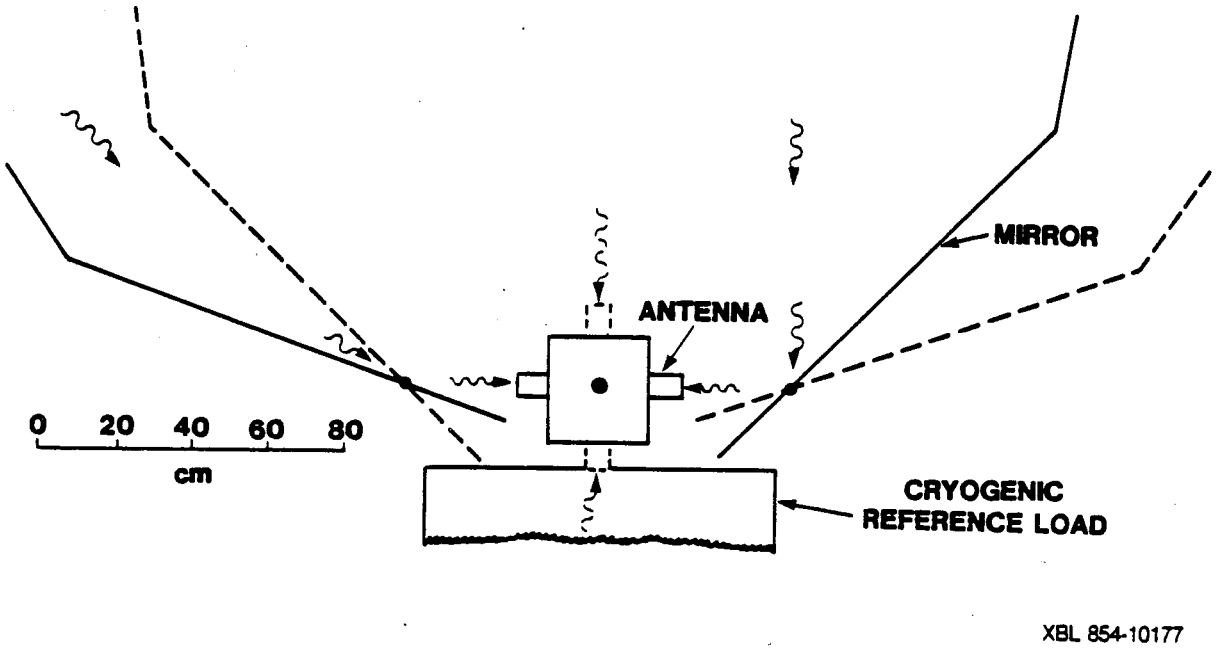

Figure 2: Schematic of the radiometer in its 1982 configuration.

Magnetic shielding around the switch and the isolator reduced the influence of the Earth's magnetic field on the radiometer's gain and offset. A heater maintained the mixer, IF amplifiers, and lockin amplifier at a constant temperature. The temperatures of the radiometer components were recorded together with the radiometer output.

The components were securely attached to a stiff mounting structure so that gravitational stresses would not cause the instrument offset to change with position. The mixer, IF amplifiers, detector diode, and lockin amplifier were all mounted on an aluminum plate. The aluminum case that housed the radiometer not only shielded the instrument from radio interference in the IF band but also formed an integral part of the structure, holding the mounting plate and the antennas securely in place.

Figure 2 shows the radiometer and its associated hardware in its 1982 configuration. The radiometer was mounted on its cart, midway between two aluminum reflectors which acted as microwave mirrors. It pivoted on bearings so that the antennas could be pointed vertically at the zenith and the cold load or horizontally to view the reflectors.

The reflectors consisted of 2.5-cm-thick sheets of foamed polyurethane, faced on both sides with sheets of aluminum. Extensions on the ends of the reflectors helped to shield the antennas from ground radiation. The reflectors could be set to allow the antennas to view the sky at nominal zenith angles of 0°, 40°, or 50°. The actual zenith angles, which differed from these nominal values by up to ~1°, were each measured to a precision of ±0°.08 (±5′) before the radiometer was transported to the observing site. The emissivity of the reflectors varied with the angle of incidence and with the polarization of the wave relative to the plane of incidence (Lorrain and Corson 1970), so the antennas were oriented with their E-plane polarization vectors 27° from horizontal in order to minimize the variation in reflector emissivity over the range of incidence angles used for zenith scans.

c) Cold Load and Ambient Calibrator

The liquid-helium (LHe) cold load used in these measurements has been described by Smoot *et al.* (1983) and by Witebsky (1985). The target, a circular disk of Eccosorb VHP-8 microwave absorber, sat at the bottom of a cylindrical, open-mouth, LHe cryostat with a 76-cm inner diameter and a depth of 130 cm. A cylinder of aluminum-coated mylar film 70 cm in diameter, concentric with the cryostat inner wall, acted as the radiometric wall. Two windows of 22-μm polyethylene film prevented air and water vapor from entering the cryostat. An aluminum plate with a circular central hole covered the top of the structure to shield the antennas from external microwave radiation and reduce the heat leak when the radiometer viewed the cold load.

The ambient calibrator, a small, styrofoam-insulated, ambient-temperature target of ferrite-loaded silicone rubber, was held in front of the antennas during measurements of the calibration coefficient G. An electronic sensor on the back allowed the target temperature to be monitored and recorded.

d) Data-Recording System

Data values from the radiometer were digitized by a 16-bit analog-to-digital converter and stored on magnetic cassette tape. The output voltages from the three Berkeley radiometers were recorded every two seconds; housekeeping data from the radiometers and cold load were recorded at sixteen-second intervals. The minimum data unit (abbreviated d.u.) for the radiometer output voltage was 0.31 mV. The output voltages and the temperature of the ambient target were also recorded by hand during measurements of the CBR temperature to provide a backup data source if the tape recorder failed.

e) Electrical Power

The radiometers, data-recording system and cold-load monitoring equipment were powered by lead-acid storage batteries connected in series to provide 24 volts. The heaters were powered by independent batteries. Both sets were charged continuously during use.

f) Measurement Procedure

The CBR measurement cycle used in 1982 consisted of the following seven steps:

1) A measurement with one antenna pointed at the zenith and the other at the cold load;

2) The same measurement, but with the radiometer rotated by 180° to reverse the antennas;

3) A gain-calibration measurement with the antennas pointed horizontally, one antenna viewing the ambient calibrator and the other viewing the zenith through a 45° reflector;

4) The same measurement with the targets interchanged;

5) A measurement of the atmosphere with the antennas pointed at the reflectors: the southward-pointing antenna viewed the zenith while the northward-looking antenna viewed the sky either 40° or 50° north of the zenith;

6) The same measurement but with the reflector settings reversed in order to scan southward;

7) A measurement in which both antennas viewed the zenith by means of the reflectors.

Steps 1 through 4 yielded the calibration coefficient and the zenith/cold-load temperature difference. Most of the atmospheric measurements (steps 5 and 6) were made at a zenith angle of 50°, but occasional measurements at 40° served as consistency checks. Step 7 was not essential to the CBR measurement, but it provided a useful check on the stability of the radiometer offset. Atmospheric measurements to both the north and the south allowed us not only to eliminate the radiometer offset but also to correct for the errors in $T_{A,\mathrm{Atm}}$ that resulted from inaccurate leveling of the radiometer cart.

IV. SYSTEM OPERATION: 1982

a) Radiometer Performance

The 3.3-mm radiometer underwent a series of tests to measure its performance and stability. The radiometer noise temperature, measured with targets at 295 K and 77 K, was 1530±20 K; the system noise fluctuations measured at White Mountain were 100±2 mK for a 2-second integration period. The radiometer offset was -7.1 ± 0.2 K. The detector diode had a nonlinearity of less than 1% for output voltages within its operating range. The offset change induced by a 1 Gauss change in the magnetic field was less than 1.5 mK. We were unable to measure the gravitationally induced offset change with the antennas pointed vertically, but our tests set a 30 mK upper limit on the change in offset when the radiometer was shifted between its two horizontal orientations.

Tests to determine the amount of ground radiation entering the antennas during atmospheric measurements set an 8 mK upper limit on $T_{\mathrm{Gnd,Atm}}$, the contribution of ground radiation to the atmospheric emission measured at zenith angles of 40° or 50°. During measurements of the zenith temperature, the estimated ground contribution, $T_{\mathrm{Gnd,Zenith}}$, was less than 1 mK.

b) 1982 Observations

Following a full-scale test of the radiometers, data-acquisition system, and cold-load assembly in Berkeley on 1982 June 14, we transported the equipment to White Mountain. In the field, the aluminum sheets on the reflectors gradually warped outward from the foamed panels to which they had been attached. This warping, which was probably the result of thermal cycling, limited our pointing accuracy during atmospheric measurements and thus caused a large uncertainty in our measurements of $T_{A,\mathrm{Atm}}$.

Measurements of T_{CBR} on July 5 lasted from 08:43 to 09:35 UT. A second series of measurements started on July 6 at 02:02 UT (near sunset) and ended at 02:58; a third series on the same date lasted from 09:06 to 09:40 UT.

V. SYSTEM OPERATION: 1983 AND 1984

The shortcomings of the original design prompted us to make several major changes in the radiometer prior to our 1983 measurements. The most fundamental of these was the reduction of the opening angle between the antennas from 180° to 60°, which enabled us to measure the atmospheric emission by pointing the antennas themselves. We rotated the radiometer to point the antennas to various pairs of zenith angles, each pair separated on the sky by approximately 60°. By eliminating the tilting reflectors, we increased both the speed and the pointing accuracy of our atmospheric measurements. The modified system is shown schematically in Figure 3.

a) Measurement Procedure

We also revised the steps in the measurement cycle to increase our data-collection efficiency. The revised measurement cycle was similar to the one used in 1982, but many of the steps were reduced to 16 seconds in length and an extra pair of atmospheric measurements was added. The first four steps in the nine-step cycle measured T_{Zenith} and the calibration coefficient G. In the first step, one antenna viewed the zenith in the reflector while the other looked into the cold load. In the second, the ambient calibrator was placed in front of the antenna that had previously viewed the zenith, while the other antenna continued to view the cold load. The third and fourth steps were repetitions of the first two measurements, but with the radiometer rotated by 60° to reverse the roles of the two antennas.

The five remaining steps yielded $T_{A,\mathrm{Atm}}$, the atmospheric antenna temperature in the zenith direction. The radiometer was stepped through a series of angles to point the two antennas approximately 10° north and 50° south of the zenith, 20° north and 40° south, 30° north and

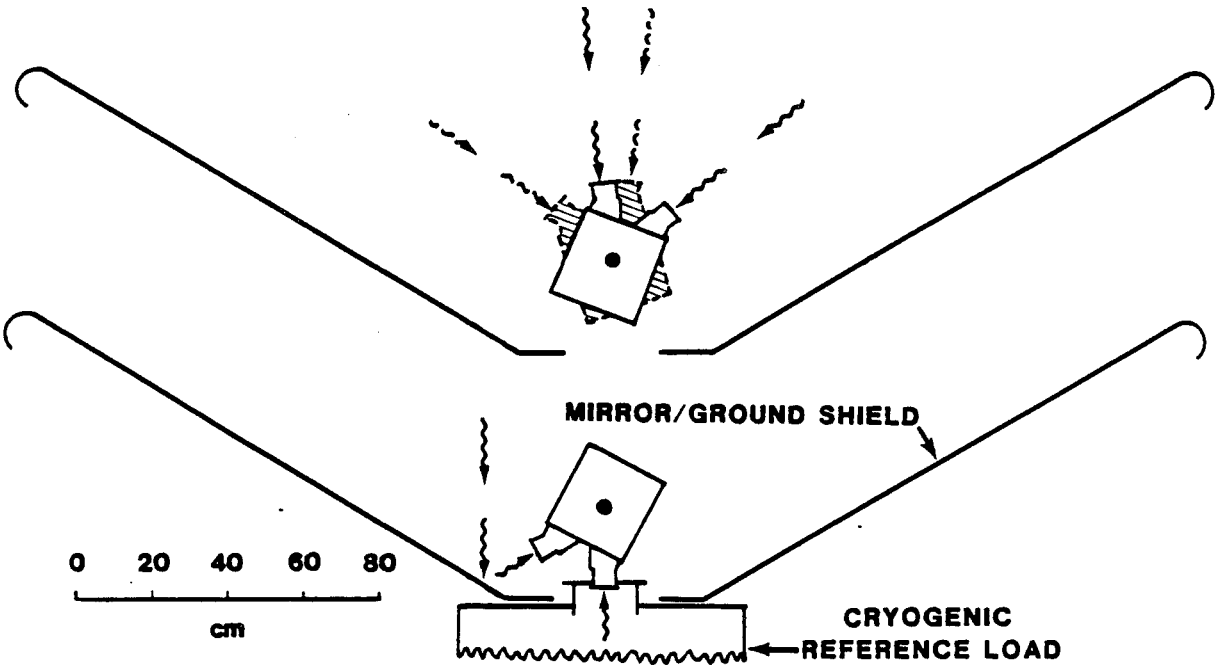

XBL 862-409

Figure 3: Schematic diagram of the radiometer and reflectors in their 1983 configuration.

30° south, 40° north and 20° south, and 50° north and 10° south, in sequence (The zenith angles quoted here are nominal values. The actual zenith angles differed from these by ~0.5°.) Two independent measurements of $T_{A,\mathrm{Atm}}$ were obtained from the pair of observations at 50° and 10° and the pair at 40° and 20°. The 30°/30° measurements enabled us to monitor the radiometer offset. A full measurement cycle lasted 192 seconds.

b) System Tests and Characteristics

The reflectors shown in Figure 3 enabled one antenna to view the zenith while the other looked into the cold load. Their thermal emission increased the antenna temperature by an amount T_{Refl}, so we measured this term in order to correct for it. To do so, we attached an insulated ambient-temperature reference load to one antenna and recorded the output voltages when the other antenna was pointed first at the reflector, where it received both the reflected radiation from the zenith and the radiation emitted by the reflector, and then directly at the zenith itself. The radiometer exhibited a small (<0.1%) position-dependent gain variation, so we repeated the measurements with the reference load cooled to 80 K. By using reference loads at two temperatures, we were able to measure the gain variation and correct for it. The tests yielded temperatures of 281 ± 22 mK and 364 ± 22 mK for the two reflectors. In a third test, we measured the output voltage with one antenna pointed directly upward and the other viewing the zenith in a small reflector mounted beside the antenna. We then interchanged the targets and repeated the measurement. The antenna temperature of the reflector was obtained from the difference in the two voltages. When this value was corrected for the incidence angle, the resulting temperature was 293 ± 16 mK.

The three tests yielded the value $T_{\mathrm{Refl}} = 312 \pm 45$ mK, where the quoted error is the rms spread. This is somewhat higher than the 250 mK theoretical value for a reflector of pure aluminum at a temperature of 280 K, used to view an 11 K source at an incidence angle of 30°. The high measured temperatures and the variability may have been caused by oxides or dust on

the reflector surfaces. The 45 mK measured spread was taken as the uncertainty in the emission from the reflectors.

The previous year's reflectors were converted to ground shields, and further shielding was added. Tests of the ground-shield performance gave a value of 12 ± 15 mK for $T_{\mathrm{Gnd,Zenith}}$ in the new radiometer configuration. They set a 27 mK upper limit on the amount of ground radiation diffracting past the edge of the shield into the antenna during atmospheric measurements 50° from the zenith.

Accurate measurements of $T_{A,\mathrm{Atm}}$ required precise values of two angles: the angle through which the radiometer rotated during the scan and the angular separation between the beam centers of the two antennas. A clinometer provided values of the rotation angle accurate to $\pm 0.^{\circ}02$ ($\pm 1'$). The antenna beam separation, measured both mechanically and radiometrically, was $59.^{\circ}57 \pm 0.^{\circ}07$.

To determine the offset change during zenith-temperature measurements, we mounted a pair of Eccosorb targets saturated with liquid nitrogen (LN) over the antenna mouths and shifted the radiometer repeatedly between the two measurement positions until differential warming caused the output voltage to drift appreciably. A fitting routine removed the drift from the data and computed the average values at the two positions. The combined result of six such tests yielded the zenith-temperature offset change: $\Delta T_{\mathrm{Offset,Zenith}} = 20 \pm 17$ mK.

We also tested for position-dependent changes in the offset temperature during measurements of $T_{A,\mathrm{Atm}}$. A pair of stable, low-reflectivity, LN-cooled loads was affixed to the mouths of the two antennas and the output voltage was recorded as the radiometer was moved repeatedly from one angle setting to another. Our tests yielded a value of 13.4 ± 9.9 mK for $\Delta T_{\mathrm{Offset,40/20}}$, the offset change during atmospheric measurements at zenith angles of 40° and 20°, and a 10.0 ± 12.6 mK value for $\Delta T_{\mathrm{Offset,50/10}}$. In both cases, the offset was larger when the radiometer was tipped northward.

Once again, we tested the system to determine whether external magnetic fields affected the offset temperature. We found the magnetically induced offset shift to be less than 5 mK/Gauss.

c) 1983 Observations

In 1983 August we returned to the observing site for another set of measurements. On the nights of September 4, 5, and 6 (UT) we measured T_{CBR} at 3.3 mm. Two observation runs on September 4 lasted 43 and 40 minutes. A 45-minute observing run occurred on September 5; another one lasting 40 minutes took place on September 6.

d) 1984 Observations

The radiometer tests were repeated prior to the 1984 observations. The measured system characteristics were essentially unchanged from those of the previous year. An extended period of bad weather at the field site hampered our observing efforts, but the weather ultimately improved enough to allow two observing runs of 60 minutes and 48 minutes on August 24 (UT) and another two, lasting 43 and 31 minutes, on August 25 (UT).

VI. DATA REDUCTION AND PROCESSING

a) Selecting and Editing the Data

Data from the observations are transferred from cassette tapes to computer for reduction and processing. Each record is examined for erroneous values: if the antennas viewed the wrong angles during a zenith scan, for example, the measurement cycle is rejected. Erroneous records result in the rejection of 5 out of 37 CBR measurement cycles in 1982, 2 out of 51 cycles in 1983, and 0 out of 57 cycles in 1984.

Output voltages recorded while the radiometer was between positions are also identified by inspection. These are discarded, and the remaining values at the position are averaged. The procedure is repeated for each step in the cycle and for all of the cycles in the observing run.

The data from 1984 suffer from an additional problem—a faulty detector diode caused the radiometer calibration coefficient to vary at the 1% level, changing abruptly and unpredictably to a new value and then returning to the old one a short time later. The gain stability becomes progressively worse from one observing run to the next. To salvage the data, we examine the output voltages from each measurement cycle for signs of abrupt gain changes and reject those cycles that show evidence of such changes. This procedure results in the loss of 0 out of 19 measurements from the first run, 3 of 15 from the second, 7 of 13 from the third, and all 10 measurements from the fourth run. Subtler gain fluctuations during the remaining cycles may have increased the statistical spread in the measured temperatures.

b) Determining the Calibration Coefficient

For the 1983 and 1984 observations, we use the equation

$$G = 2\,\frac{T_{A,\mathrm{Amb}} - T_{A,\mathrm{Load}}}{V_{\mathrm{Amb/Load}} - V_{\mathrm{Load/Amb}}}$$

to derive the calibration coefficient, G, for each measurement cycle. The terms $T_{A,\mathrm{Amb}}$ and $T_{A,\mathrm{Load}}$ are the antenna temperatures of the ambient calibrator and cold load. The values $V_{\mathrm{Amb/Load}}$ and $V_{\mathrm{Load/Amb}}$ are the radiometer output voltages recorded during steps 2 and 4 of the cycle under consideration. They are differenced in order to remove the radiometer offset. The equation used G in 1982 is similar, with slight differences caused by the more complex gain-calibration procedure used that year. Values of G for the three years fall in the range from 8.8 to 10.5 mK/data unit.

c) Determining the Zenith Temperature

The equation used to calculate T_{Zenith} from the 1983 and 1984 measurements is

$$T_{\mathrm{Zenith}} = \frac{G}{2}(V_{\mathrm{Zenith/Load}} - V_{\mathrm{Load/Zenith}}) - \frac{\Delta T_{\mathrm{Offset,Zenith}}}{2} + T_{A,\mathrm{Load}} - T_{\mathrm{Refl}}\,. \qquad (2)$$

The value of the offset shift $\Delta T_{\mathrm{Offset,Zenith}}$, derived in § V*b*, is 20 ± 17 mK. The term T_{Refl} is the antenna temperature of the reflectors in which the antennas view the zenith. The radiative contributions from the target, the windows, the walls, and other sources which constitute $T_{A,\mathrm{Load}}$ are discussed in detail in Appendix A. The equation used to derive T_{Zenith} from the 1982 measurements does not include a correction for T_{Refl} because the antennas viewed the zenith directly. The value of $\Delta T_{\mathrm{Offset,Zenith}}$ in 1982 is discussed in § VII*b*.

d) Determining $T_{A,\mathrm{Atm}}$

Each value of $T_{A,\mathrm{Atm}}$ is derived from two temperature-difference measurements. The output voltage measured at one pair of nominal zenith angles (e.g. 10° north and 50° south) is subtracted from the voltage measured at the complementary pair of angles (50° north and 10° south) to remove the radiometer offset. The difference in the antenna temperatures at the nominal zenith angles θ_1 and θ_2 is calculated by means of the formula:

$$\Delta T_{\mathrm{Sky},\theta_1/\theta_2} = \frac{1}{2}\left[G\left(V_{\theta_1/\theta_2} - V_{\theta_2/\theta_1}\right) - \Delta T_{\mathrm{Offset},\theta_1/\theta_2}\right] - T_{\mathrm{Gnd,Atm}}, \qquad (3)$$

where $T_{\mathrm{Gnd,Atm}}$ is the contribution from ground radiation and $\Delta T_{\mathrm{Offset},\theta_1/\theta_2}$ is the position-dependent offset change.

The radiometric sky temperature at zenith angle Z is determined by the physical temperature and emissivity of the atmosphere at Z. The sky temperature varies roughly as $\sec(Z)$, but atmospheric self-absorption and the finite width of the antenna pattern cause its behavior to depart significantly from a secant law. One can use the measured value of $\Delta T_{\mathrm{Sky},\theta_1/\theta_2}$, together with a model of the atmospheric temperature and air-mass distributions described in Appendix B, to determine the zenith opacity, τ_0. Using this value and the model, one can then compute $T_{A,\mathrm{Atm}}$. Although the atmospheric temperature differences are subscripted with the nominal zenith angles, θ_1 and θ_2, the atmospheric model uses the actual measured zenith angles Z_1 through Z_4.

Dividing the temperature difference $\Delta T_{\mathrm{Sky},\theta_1/\theta_2}$ by $\Delta\Gamma_1$, a quantity roughly equal to the product of the physical temperature of the atmosphere and the difference $[\sec(\theta_1) - \sec(\theta_2)]$, one obtains ϵ, a term approximately equal to τ_0. One then calculates $T_{A,\mathrm{Atm}}$ from the equation

$$T_{A,\mathrm{Atm}} \approx \epsilon\, T_{\mathrm{Atm},1} + \epsilon^2\, T_{\mathrm{Atm},2} + \epsilon^3\, T_{\mathrm{Atm},3}\ . \tag{4}$$

Equation (4) and the terms $T_{\mathrm{Atm},1}$, $T_{\mathrm{Atm},2}$, $T_{\mathrm{Atm},3}$, and $\Delta\Gamma_1$ are derived in Appendix B. The first-order term in equation (4) represents the value of $T_{A,\mathrm{Atm}}$ before corrections for atmospheric self-absorption. Its value is independent of the physical temperature assumed by the atmospheric model. The higher-order terms are self-absorption corrections, typically ~300 mK total.

Atmospheric measurements from all three years are processed similarly. The only significant changes occurred in 1983, when the nominal zenith angles were altered and the number of atmospheric measurements was increased from two to four. The 1983/1984 cycle yields two independent measurements of $T_{A,\mathrm{Atm}}$ from the observations at 40° and 20° and those at 50° and 10°. The average of the two is used to calculate $T_{A,\mathrm{CBR}}$.

e) Determining $T_{A,\mathrm{CBR}}$

The CBR antenna temperatu. e is the difference between T_{Zenith} and $T_{A,\mathrm{Atm}}$:

$$T_{A,\mathrm{CBR}} = T_{\mathrm{Zenith}} - T_{A,\mathrm{Atm}} - T_{\mathrm{Gnd,Zenith}}\ , \tag{5}$$

where $T_{\mathrm{Gnd,Zenith}}$ is the ground radiation entering the upward-pointing antenna. The values of $T_{A,\mathrm{CBR}}$ from all the measurement cycles of an observing run are averaged. Tables 1, 2, and 3 contain the mean values of $T_{A,\mathrm{CBR}}$, G, T_{Zenith}, and $T_{A,\mathrm{Atm}}$ from all the observing runs. The mean values of $T_{A,\mathrm{CBR}}$ from each observing run of a given year are combined to form an overall average for that year, $\langle T_{A,\mathrm{CBR}} \rangle$. How the averages are formed is a topic discussed in § VII, which deals with error analysis.

TABLE 1

Results of the 1982 CBR Measurements[a]

Date Time	θ	Number of Observations	G (mK/du)	T_{Zenith} (K)	$T_{A,Atm,1}$ (K)	$T_{A,Atm,2}$ (K)	$T_{A,CBR,1}$ (K)	$T_{A,CBR,2}$ (K)
Jul 5 08:46–09:20	40°	3	...	...	12.648 ±0.207	12.228 ±0.200	0.549 ±0.195	0.970 ±0.188
...	50°	6	...	...	12.236 ±0.167	11.256 ±0.153	0.974 ±0.193	1.954 ±0.179
...	both	9	9.716 ±0.010	13.206 ±0.026	...	...	...	...
Jul 6 02:02–02:59	40°	3	...	...	14.227 ±0.474	13.752 ±0.458	0.535 ±0.092	1.009 ±0.080
...	50°	11	...	...	13.995 ±0.538	12.870 ±0.493	0.506 ±0.561	1.631 ±0.523
...	both	14	10.469[b] ±0.034	14.532 ±0.317	...	...	...	...
Jul 6 09:06–09:40	40°	3	...	... ±0.371	13.230 ±0.358	12.790 ±0.239	0.303 ±0.226	0.744
...	50°	6	...	...	13.010 ±0.350	11.967 ±0.321	0.667 ±0.242	1.711 ±0.218
...	both	9	9.768 ±0.007	13.630 ±0.182	...	...	...	...

[a]Quoted errors are rms statistical uncertainties.

[b]The high value of G results from the high setting of the temperature controller during this run.

TABLE 2

Results of the 1983 CBR Measurements[a]

Date Time	Number of Observations	G (mK/du)	T_{Zenith} (K)	$T_{A,Atm,40/20}$ (K)	$T_{A,Atm,50/10}$ (K)	$T_{A,CBR}$ (K)
Sept 4 06:33–07:14	11	8.771 ±0.007	10.561 ±0.078	9.611 ±0.147	9.550 ±0.113	0.980 ±0.089
Sept 4 11:58–12:36	12	8.752 ±0.004	10.160 ±0.090	9.167 ±0.154	9.171 ±0.087	0.991 ±0.098
Sept 5 05:23–06:08	14	9.037 ±0.037	12.004 ±0.088	10.934 ±0.168	11.051 ±0.102	1.011 ±0.117
Sept 6 05:38–06:17	12	9.171 ±0.016	13.048 ±0.207	12.210 ±0.519	12.139 ±0.456	0.873 ±0.492

[a]Quoted errors are rms statistical uncertainties.

TABLE 3

Results of the 1984 CBR Measurements[a]

Date Time	Number of Observations	G (mK/du)	$T_{\rm Zenith}$ (K)	$T_{\rm A,Atm,40/20}$ (K)	$T_{\rm A,Atm,50/10}$ (K)	$T_{\rm A,CBR}$ (K)
Aug 24 07:58–08:58	19	10.963 ±0.006	12.259 ±0.683	11.474 ±1.464	11.273 ±0.995	0.885 ±0.979
Aug 24 11:38–12:26	12	10.897 ±0.005	10.118 ±0.132	8.926 ±0.273	8.954 ±0.204	1.178 ±0.285
Aug 25 05:13–05:56	6	10.869 ±0.006	14.073 ±0.090	13.197 ±0.338	13.287 ±0.206	0.831 ±0.196

[a]Quoted errors are rms statistical uncertainties.

VII. DATA ANALYSIS—UNCERTAINTIES AND SYSTEMATIC ERRORS

The measurement uncertainty is largely determined by systematic errors. These fall into seven categories:

1) Errors in the cold-load antenna temperature;
2) Errors caused by position-dependent offset changes;
3) Errors in the corrections for reflector emissivity;
4) Errors due to ground radiation;
5) Errors in the radiometer calibration;
6) Errors in the atmospheric model;
7) Pointing errors during atmospheric measurements.

Tables 4 and 5 list the terms that enter into the computation of $T_{A,\rm CBR}$ and the estimated systematic errors associated with each term. The overall systematic uncertainties are quadrature sums of the entries in the tables. Statistical uncertainties are small compared to systematics in the 1982 and 1983 measurements, but they comprise a significant fraction of the 1984 error budget.

a) Cold-Load Uncertainties

From Appendix A, the estimated value of $T_{A,\rm Load}$ is 2083 ± 37 mK, so the resulting uncertainties in $T_{\rm Zenith}$ and $T_{A,\rm CBR}$ are ±37 mK. The small error in G that results from the uncertainty in $T_{A,\rm Load}$ is discussed in the section on calibration-related errors.

b) Offset Changes

Tests in 1982 set a 30 mK upper limit on the position-dependent offset shift with the radiometer pointed horizontally, but do not indicate whether the offset changes when the instrument is shifted between vertical positions. Analysis of the 1982 CBR-measurement data reveals a change of 16 ± 16 mK between the vertical and horizontal offsets. (The 300 mK offset change reported by De Amici *et al.* [1984] is incorrect because the analysis did not fully correct for the zenith/cold-load temperature difference.) Neither of these results rules out large offset variations during zenith measurements, but they do suggest that any changes are probably smaller than ~100 mK. If this value is adopted as a conservative estimate of the uncertainty in $\Delta T_{\rm Offset,Zenith}$, the resulting uncertainty in $T_{\rm Zenith}$ is ±50 mK.

TABLE 4

Systematic Errors and Correction Terms: 1982

Term	Value	Source of Error	Error Value	Error in $T_{A,\mathrm{CBR}}$
		Calibration		
G	9.70 to 10.54 mK/du			
		Gain Drift	±0.07%	±8 mK
		Calibration-Load Uncertainties	±0.65%	±10 mK
		Angular dependence	±0.1%	±12 mK
		Nonlinearity	±1.1%	±17 mK
		Total:	±1.3%	±24 mK
		T_{Zenith}		
$\Delta T_{\mathrm{Offset,Zenith}}$	0 mK	Offset Changes	±100 mK	±50 mK
$T_{\mathrm{Gnd,Zenith}}$	0 mK	Ground Radiation	$^{+1}_{-0}$ mK	$^{+0}_{-1}$ mK
$T_{A,\mathrm{Load}}$:				
$T_{A,\mathrm{Target}}$	2020 mK	Temperature Uncertainty	±4 mK	
$T_{A,\mathrm{Windows}}$	53 mK	Window Emission and Reflection	±35 mK	
$T_{A,\mathrm{Wall}}$	10 mK	Wall Temperature and Emissivity	±10 mK	
Total:	2083 mK		±37 mK	±37 mK
		$T_{A,\mathrm{Atm}}$		
$T_{\mathrm{Gnd,Atm}}$	0 mK	Ground Radiation	$^{+8}_{-0}$ mK	$^{+22}_{-0}$ mK
T_{Refl}	285 mK	Reflector Emission	±45 mK	±45 mK
Pointing Errors:				
Type 1		Cart Tilt	±1°	±30 mK
Type 2		Antenna Misalignment	±0.°17	±115 mK
Type 4		Reflector Misalignment	±1°	±550 mK
Modeling Errors:		Atmospheric Temperature and Emissivity Profiles		±26 mK
			Total:	±570 mK

TABLE 5

Systematic Errors and Correction Terms: 1983 and 1984

Term	Value	Source of Error	Error Value	Error in $T_{A,\mathrm{CBR}}$
		Calibration		
G	8.75 to 9.20 mK/du			
		Gain Drift	±0.09%	±11 mK
		Calibration-Load Uncertainties	±0.65%	±10 mK
		Angular dependence	±0.1%	±12 mK
		Nonlinearity	±1.1%	±17 mK
		Total:	±1.3%	±26 mK
		T_{Zenith}		
$\Delta T_{\mathrm{Offset,Zenith}}$	20 mK	Offset Changes	±17 mK	±9 mK
$T_{\mathrm{Gnd,Zenith}}$	12 mK	Ground Radiation	±15 mK	±15 mK
T_{Refl}	312 mK	Reflector Emission	±45 mK	±45 mK
$T_{A,\mathrm{Load}}$:				
$T_{A,\mathrm{Target}}$	2020 mK	Temperature Uncertainty	±4 mK	
$T_{A,\mathrm{Windows}}$	53 mK	Window Emission and Reflection	±35 mK	
$T_{A,\mathrm{Wall}}$	10 mK	Wall Temperature and Emissivity	±10 mK	
Total:	2083 mK		±37 mK	±37 mK
		$T_{A,\mathrm{Atm}}$		
$T_{\mathrm{Gnd,Atm}}$	0 mK	Ground Radiation	$^{+15}_{-0}$ mK	$^{+30}_{-0}$ mK
$\Delta T_{\mathrm{Offset,40/20}}$	−13 mK	Offset Changes	±10 mK	±21 mK
$\Delta T_{\mathrm{Offset,50/10}}$	−10 mK	Offset Changes	±13 mK	±12 mK
Pointing Errors:				
Type 1		Cart Tilt	±0°.50	±12 mK
Type 2		Antenna Misalignment	±0°.07	±40 mK
Type 3		Inaccurate Positions	±0°.03	±16 mK
Modeling Errors:		Atmospheric Temperature and Emissivity Profiles		±26 mK
				Total: ±90 mK

Offset changes cause uncertainty in both the zenith and atmospheric measurements in 1983 and 1984. The 20 ± 17 mK value of $\Delta T_{\mathrm{Offset,Zenith}}$ gives rise to a ± 9 mK uncertainty in T_{Zenith}. Uncertainty in $\Delta T_{\mathrm{Offset},\theta_1/\theta_2}$ (-13 ± 10 mK for $40°/20°$ atmospheric measurements and -10 ± 13 mK for $50°/10°$ measurements) causes estimated errors of ± 21 mK in $T_{A,\mathrm{Atm},40/20}$ and ± 12 mK in $T_{A,\mathrm{Atm},50/10}$.

c) Reflector Emission

In the 1982 configuration, the radiometer views the reflectors only during atmospheric and calibration measurements. The emissivity variation over the reflector surface is unknown, but if one uses the ± 45 mK value from § V*b* as a representative estimate, the change in the reflector surface area viewed by the antenna during sky measurements at the various zenith angles results in uncertainties of approximately ± 45 mK in the values of $T_{A,\mathrm{Atm}}$. The 312 ± 45 mK value of T_{Refl} in 1983 and 1984 creates ± 45 mK uncertainties in the values of T_{Zenith} and $T_{A,\mathrm{CBR}}$ from those years.

d) Ground Radiation

Calculations indicate that the 1982 value of $T_{\mathrm{Gnd,Zenith}}$ is less than 1 mK. The 8 mK upper limit on $T_{\mathrm{Gnd,Atm}}$ in 1982 places uncertainties of 28 mK and 15 mK on values of $T_{A,\mathrm{Atm}}$ obtained from observations at 40° and 50°, respectively.

Tests yield the value 12 ± 15 mK for $T_{\mathrm{Gnd,Zenith}}$ in 1983 and 1984. The uncertainty in this term contributes directly to the error in $T_{A,\mathrm{CBR}}$. The 27 mK upper limit on $T_{\mathrm{Gnd,Atm}}$ for observations at 50° causes a $^{+49}_{-0}$ mK uncertainty in $T_{A,\mathrm{Atm},50/10}$ in 1983 and 1984. Similar measurements have not been performed at 40°, but calculations indicate that the uncertainty in $T_{A,\mathrm{Atm},40/20}$ due to ground radiation is smaller than $^{+11}_{-0}$ mK. When the measurements at both sets of zenith angles are averaged, the error in $T_{A,\mathrm{Atm}}$ caused by ground radiation is $^{+30}_{-0}$ mK.

e) Gain Calibration and Linearity

Calibration errors can occur if the radiometer gain drifts significantly during a measurement cycle, if the gain changes systematically from one radiometer position to another, if measurements of the calibration coefficient are inaccurate, or if the radiometer response is nonlinear.

The maximum error in $T_{A,\mathrm{CBR}}$ due to gain drifts during a measurement sequence is $(\delta G/G) \times T_{A,\mathrm{Atm}}$, where $\delta G/G$ is the fractional gain drift between the zenith and atmospheric measurements. The calibration and atmospheric-temperature data yield conservative upper limits of ± 8 mK, ± 11 mK, and ± 8 mK on the error in $T_{A,\mathrm{CBR}}$ resulting from systematic gain drifts in 1982, 1983, and 1984 respectively. The position-dependent gain modulation mentioned in § V can be treated similarly: a 10^{-3} calibration change between the measurements of T_{Zenith} and $T_{A,\mathrm{Atm}}$ causes a ± 13 mK error in $T_{A,\mathrm{CBR}}$. Residual gain fluctuations in the 1984 data (§ VI*a*) are assumed to contribute to the variation in the measured values of $T_{A,\mathrm{CBR}}$ and are treated as part of the statistical error.

A stable but poorly measured calibration coefficient causes errors in T_{Zenith} and $T_{A,\mathrm{Atm}}$ that nearly cancel each other, so the error in $T_{A,\mathrm{CBR}}$ is small. One can show from equations (2), (3), (4), and (5) that a fractional error $\delta G/G$ in the calibration coefficient causes $T_{A,\mathrm{CBR}}$ to be in error by less than $1.4\,(\delta G/G)$ K. Our knowledge of the antenna temperatures of the cold and ambient loads limits the calibration accuracy to $\pm 0.65\%$ and adds ± 9 mK to the uncertainty in $T_{A,\mathrm{CBR}}$.

One can verify the linearity of the radiometer's response by comparing the gain calibrations made using targets at a variety of temperatures. The 1983 observations include radiometer calibrations made with ambient and LN-cooled targets as well as the usual ambient/LHe calibrations. These data can be combined to yield the average calibration coefficient for targets with antenna

temperatures between 2.1 K (LHe) and 71.6 K (LN) instead of an ambient-temperature target and a cold one. The resulting coefficient differs by only 1.1% from the calibration coefficient measured with ambient and LN-cooled targets, a discrepancy compatible with the uncertainties in the calibrations themselves. Nonlinearity thus affects G by less than 1.1% over the range of temperatures viewed by the radiometer during CBR measurements and causes an error of less than ± 17 mK in $T_{A,\mathrm{CBR}}$.

The net result of the various calibration uncertainties is that the measured calibration coefficient G is in error by no more than $\pm 1.3\%$ and that it drifts by no more than $\pm 0.1\%$ between measurements. These uncertainties give rise to an estimated error of ± 23 mK in $T_{A,\mathrm{CBR}}$.

f) Atmospheric-Model Uncertainties

The atmospheric model contains data describing the antenna gain pattern and the temperature and emissivity profiles of the atmosphere. If the model values deviate from the actual characteristics, errors in $T_{A,\mathrm{Atm}}$ result.

When three independent evaluations of the gain pattern are used in the model, the resulting values of $T_{A,\mathrm{Atm}}$ differ by ± 6 mK. This value is taken as the uncertainty in $T_{A,\mathrm{Atm}}$ due to errors in the gain pattern.

The atmospheric-temperature profile used for the calculations is discussed in Appendix B. The quantitative details of the model temperature profile have little effect on the computed value of $T_{A,\mathrm{Atm}}$ because the atmospheric temperature only enters into corrections for self-absorption. An overall error of ± 10 K in the temperature profile causes a ± 16 mK error in $T_{A,\mathrm{Atm}}$. If the temperature profile is replaced by a uniform, emissivity-weighted average atmospheric temperature, the computed value of $T_{A,\mathrm{Atm}}$ changes by less than 7 mK.

The densities of oxygen and water vapor, the two atmospheric components that produce most of the radiation at 3.3 mm, both decrease approximately exponentially with altitude, but the scale heights differ for the two gases: typical scale heights are 9.5 km for oxygen and 2.2 km for water vapor. If the scale heights for oxygen and water vapor are each used to compute $T_{A,\mathrm{Atm}}$, the resulting temperatures differ by 38 mK or less. The assumed value of $T_{A,\mathrm{Atm}}$ is the average of the two values, and the estimated error due to uncertainty in the effective scale height is half the difference, ± 19 mK.

The overall uncertainty in $T_{A,\mathrm{Atm}}$ due to model-related errors is the quadrature sum of the individual error terms, ± 26 mK. This same error also contributes to the overall uncertainty in $T_{A,\mathrm{CBR}}$.

g) Pointing Errors

Pointing errors can be divided into four categories according to the way that the errors at the four zenith angles are correlated:

1) Equal and opposite errors for northward- and southward-looking observations (cart tipping in the north-south plane, for example). Although pointing errors of this type can be as large as $\sim 1°$, they have little effect on $T_{A,\mathrm{Atm}}$ because the errors to the north and south cancel to first order.

2) Errors having the same value and sign for observations to the north and south (e.g. those due to as inaccurate measurement of the beam separation between the two antennas).

3) Equal and opposite errors in two zenith angles—Z_1 and Z_3, or Z_2 and Z_4—with no associated error in the other two zenith angles. These could have occurred in the 1983/1984 configuration if the radiometer orientation were incorrectly measured in one or more scan positions.

4) Errors that occur at one zenith angle and are not correlated with errors elsewhere (e.g. poorly measured reflector settings in the 1982 configuration).

This division is useful for the analysis because the effect of pointing errors on $T_{A,\mathrm{Atm}}$ depends on their correlation as well as on their magnitude.

North-south cart tilt in 1982 causes a Type-1 pointing error of up to 1° and leads to a ±30 mK error in $T_{A,\mathrm{Atm}}$. A type-2 pointing error in the form of a ±0.°17 uncertainty in the antenna alignment results in an additional ±115 mK of uncertainty. Type-3 pointing errors are of little consequence due to the radiometer design, but the type-4 error associated with the uncertainty in the reflector settings is responsible for most of the uncertainty in the 1982 atmospheric measurements. The angles measured before and after the observations differ by as much as 2.°3 because of reflector warp and measurement inaccuracy. Neither set of values is trustworthy, so the observations are analyzed using both sets. This analysis yields two values of $T_{A,\mathrm{Atm}}$ from each measurement cycle: one value, subscripted 1, derived using the the first set of angle measurements, and a second value, subscripted 2, computed from the second set. The two values of $T_{A,\mathrm{CBR}}$ are subscripted similarly. There is no *a priori* reason to give preference to either set of angle measurements, to believe that one night's values of $T_{A,\mathrm{Atm}}$ are more accurate than the other's, or to favor the results of atmospheric measurements at either 40° or 50°. We therefore compute values of $T_{A,\mathrm{CBR}}$ using both sets of angle factors and average the results from both nights. The four values of $T_{A,\mathrm{CBR}}$ listed in Table 1 for 1982 July 5 are treated independently of one another. Because of the systematic shift in the values of $T_{A,\mathrm{CBR}}$ from July 5 to July 6, the results from the two runs on July 6 are averaged so that each is given half the weight of the single run on July 5. The spread in the values of $T_{A,\mathrm{CBR}}$ derived in the various ways provides an estimate of the type-4 pointing error in $T_{A,\mathrm{Atm}}$ due to errors in the zenith angles. The mean of the eight temperature values from the three runs is 1.00 K. The 0.55 K standard deviation in the values is taken as the uncertainty caused by type-4 pointing errors. The total uncertainty in $T_{A,\mathrm{Atm}}$ and $T_{A,\mathrm{CBR}}$ due to pointing errors is ±0.56 K, the quadrature sum of the uncertainties due to type-1, type-2, and type-4 pointing errors.

The pointing errors are greatly reduced in the 1983 and 1984 measurements because moveable reflectors are not used. Type-1 pointing errors cause uncertainties of ±11 mK in values of $T_{A,\mathrm{Atm}}$ measured at 40°/20° and ±13 mK in those measured at 50°/10°. The only significant type-2 pointing error is the ±0.°07 uncertainty in the beam separation of the two antennas discussed in § V, which gives rise to a ±40 mK uncertainty in $T_{A,\mathrm{Atm}}$. A ±0.°03 uncertainty in the radiometer positions (type-3) causes errors of ±19 mK and ±12 mK in measurements of $T_{A,\mathrm{Atm}}$ made at 40°/20° and at 50°/10°, respectively. The radiometer design virtually eliminates type-4 pointing errors. The total estimated error in the 1983 and 1984 measurements of $T_{A,\mathrm{Atm}}$ (and $T_{A,\mathrm{CBR}}$) due to pointing errors is the quadrature sum of the error estimates for pointing errors of types 1, 2, and 3, ±45 mK.

h) Statistical Fluctuations

Fluctuations in the radiometer output are primarily the result of variations in the internally-generated radiometer noise and in atmospheric emission. Irregular gain fluctuations may also have contributed to the statistical uncertainty in the 1984 measurements. The random fluctuations that constitute radiometer noise are proportional to the sum of the system noise temperature and the temperature of the target. When the output voltage is averaged for a time τ, the fluctuations integrate down as $\tau^{-1/2}$ for values of τ up to 30 minutes. Unlike the frequency-independent spectrum of radiometer noise, the atmospheric fluctuation spectrum is dominated by the large-amplitude, low-frequency drifts that occur as regions of varying water-vapor content are observed by the antennas. The amplitude of the atmospheric components drops below the level of the radiometer-noise fluctuations at periods shorter than about 120 seconds. In actual measurements of the CBR temperature, the errors caused by atmospheric fluctuations exceed those due to radiometer noise by a factor of three or more. The net effect of noise fluctuations can be seen in the rms variation in the values listed in Tables 1, 2, and 3.

The statistical error in the mean of the 1982 measurements is ±0.034 K. The average CBR antenna temperature, derived above, is $\langle T_{A,\mathrm{CBR}} \rangle = 1.00$ K. The 1983 result is a weighted average of the mean values from the four observing runs: $\langle T_{A,\mathrm{CBR}} \rangle = 0.99$ K with a ±0.016 K statistical uncertainty in the mean. Figure 4, a histogram of the CBR antenna temperatures measured on 1983 September 4 and 5, shows the distribution of values when observing conditions were especially good.

The values of $T_{A,\mathrm{CBR}}$ from the second and third observing runs of 1984 are not in statistical agreement, so the mean uncertainties from the three runs cannot be used as weighting factors. The value of the CBR antenna temperature from 1984 is a straight average of the values from the three runs, $\langle T_{A,\mathrm{CBR}} \rangle = 0.96$ K, with a mean statistical uncertainty of ±0.11 K.

i) Summary

The total estimated error in each year's result is the quadrature sum of the systematic errors (±0.57 K in 1982, ±0.09 K in 1983 and 1984) and the statistical uncertainty. The average CBR antenna temperatures from the three years are thus:

$$\langle T_{A,\mathrm{CBR}} \rangle = 1.00 \pm 0.57 \text{ K} \qquad \text{in 1982;}$$
$$\langle T_{A,\mathrm{CBR}} \rangle = 0.99 \pm 0.09 \text{ K} \qquad \text{in 1983;}$$
$$\langle T_{A,\mathrm{CBR}} \rangle = 0.96 \pm 0.14 \text{ K} \qquad \text{in 1984.}$$

VIII. RESULTS AND INTERPRETATION

The inverse of equation (1) is used to convert the yearly averages of § VII to brightness temperatures:

$$T_{\mathrm{CBR}} = 2.58^{+0.68}_{-0.79} \text{ K} \qquad \text{in 1982;}$$
$$T_{\mathrm{CBR}} = 2.57 \pm 0.12 \text{ K} \qquad \text{in 1983;}$$
$$T_{\mathrm{CBR}} = 2.53 \pm 0.18 \text{ K} \qquad \text{in 1984.}$$

The average of the three values, weighted by their *statistical* uncertainties (assumed to be independent from year to year), is 2.57 ± 0.12 K. The quoted error is the total uncertainty.

The 1982 CBR temperature quoted here is somewhat different from the previously reported value from the same measurements (De Amici *et al.* 1984), $T_{\mathrm{CBR}} = 2.42 \pm 1.00$ K. The new temperature value comes from a reanalysis of the 1982 measurements using the actual antenna gain pattern instead of a Gaussian model. This correction reduces measured values of $T_{A,\mathrm{Atm}}$ by 140 mK and increases T_{CBR} by 160 mK. The overestimate of the uncertainty in the CBR temperature, mentioned in § VII*b*, has also been corrected.

a) Comparison with Previous and Related Measurements

Table 6 lists the results of our CBR measurements at all five wavelengths. The individual brightness temperatures and their weighted mean, 2.72 ± 0.04 K, are consistent with the 3.3 mm value.

The value at 3.3 mm is in good agreement with a variety of other CBR temperature measurements in the same wavelength range. Previous heterodyne measurements near 3.3 mm have a weighted mean of 2.55 ± 0.19 K (Boynton *et al.* 1968; Kislyakov *et al.* 1971; Millea *et al.* 1971; Boynton and Stokes 1974). Weiss (1980) summarizes these and other CBR measurements.

Peterson, Richards, and Timusk (1985) have measured T_{CBR} in five wavelength bands using a balloon-borne cryogenic multichannel bolometer. In the wavelength range from 2.95 to 4.35 mm, they report a temperature of 2.80 ± 0.16 K. Spectroscopic measurements of CN molecules in the directions of ζ Ophiuchi, ζ Persei, and o Persei by Meyer and Jura (1985) yield CBR temperatures

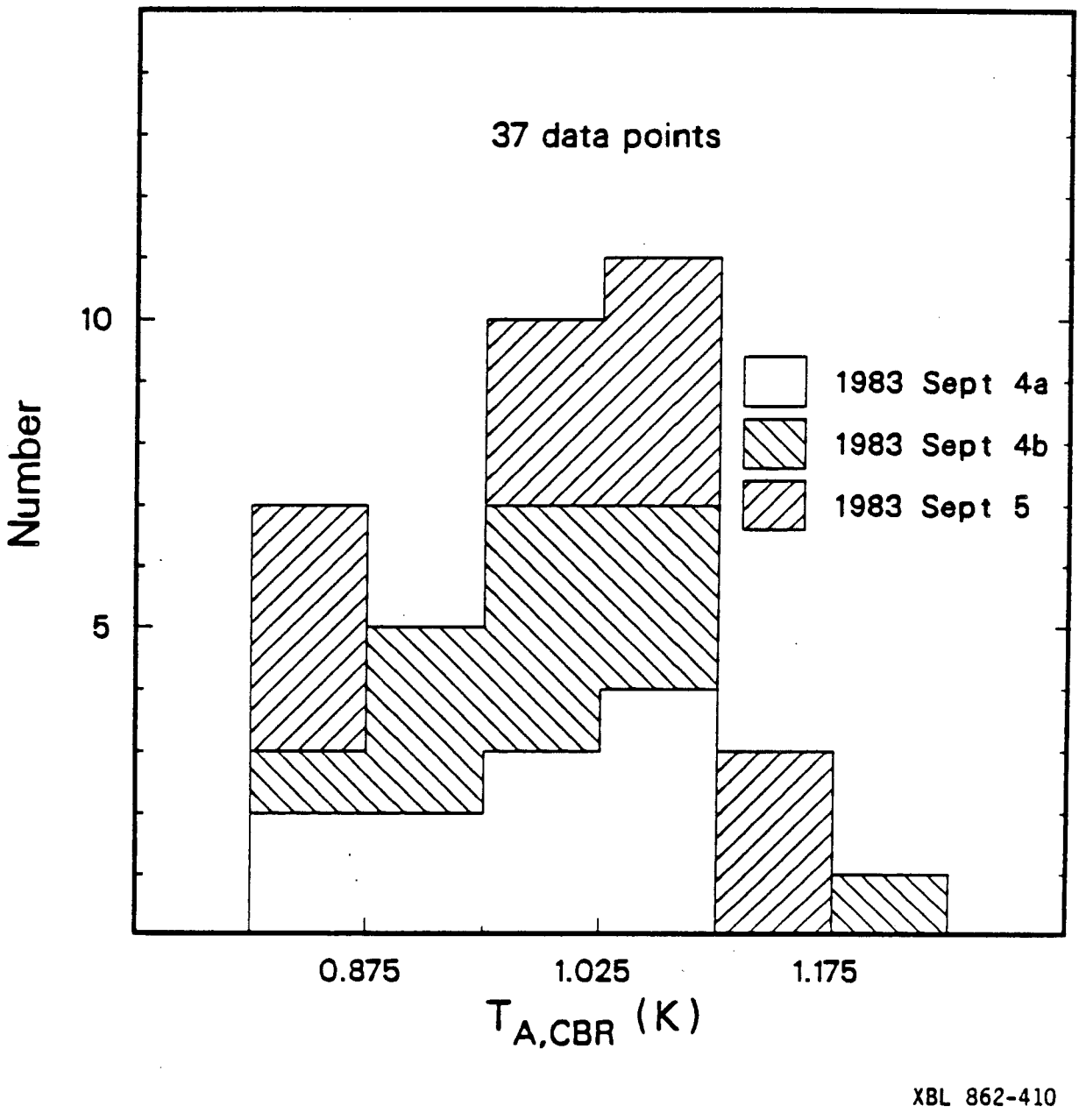

Figure 4: Histogram of CBR measurements at 3.3 mm on 1983 September 4 and 5.

TABLE 6

Results of Our CBR Temperature Measurements[a]

Wavelength (cm)	Number of Observations	$T_{A,\mathrm{Atm}}$ (K)	$T_{A,\mathrm{CBR}}$ (K)	T_{CBR} (K)	Combined Results[b]
12.0	6	0.95 ± 0.05	2.49 ± 0.24	2.55 ± 0.24	2.78 ± 0.13
	18	0.95 ± 0.05	2.82 ± 0.15	2.88 ± 0.16	
6.3	5	1.0 ± 0.1	2.64 ± 0.21	2.74 ± 0.22	2.71 ± 0.08
	38	1.00 ± 0.07	2.60 ± 0.08	2.71 ± 0.08	
	82	0.93 ± 0.16	2.68 ± 0.17	2.91 ± 0.17	
3.0	59	1.20 ± 0.13	2.41 ± 0.14	2.64 ± 0.14	2.75 ± 0.08
	34	1.15 ± 0.09	2.46 ± 0.10	2.70 ± 0.13	
	21	4.85 ± 0.14	2.10 ± 0.20	2.82 ± 0.21	
0.91	32	4.53 ± 0.09	2.09 ± 0.13	2.81 ± 0.14	2.81 ± 0.12
	36	4.34 ± 0.09	2.09 ± 0.13	2.81 ± 0.14	
	29	12.6 ± 0.59	1.00 ± 0.57	$2.58^{+0.68}_{-0.79}$	
0.33	49	9.87 ± 0.09	0.99 ± 0.09	2.57 ± 0.12	2.57 ± 0.12
	44	11.3 ± 0.13	0.96 ± 0.14	2.53 ± 0.18	

[a] The three rows at each wavelength list the results from 1982, 1983, and 1984 in order. The quantities $T_{A,\mathrm{CBR}}$ and T_{CBR} are the CBR antenna temperature and brightness temperature, respectively. The quoted errors are 68% confidence level limits.

[b] The combined results are weighted averages of the measured T_{CBR} values from the three years.

of 2.70 ± 0.04 K at 2.64 mm and 2.76 ± 0.20 K at 1.32 mm. Our 3.3 mm result, combined with the value reported by Meyer and Jura at 2.64 mm, the Peterson, Richards, and Timusk result at 2.95 to 4.35 mm, and the previous heterodyne measurements near 3.3 mm, fit a 2.69 ± 0.04 K blackbody spectrum. The χ^2 is 2.3 for 6 degrees of freedom, indicating a good fit to the blackbody model.

On the other hand, earlier bolometric measurements by Woody and Richards (1979, 1981) using a balloon-borne Fourier spectrometer yield CBR temperatures of $3.28^{+0.29}_{-0.23}$ K at 4.20 mm and $3.09^{+0.20}_{-0.14}$ K at 2.94 mm, in poor agreement with the 2.57 ± 0.12 K result reported here and with the CN measurements. This disagreement casts doubt upon the apparent evidence for spectral distortions reported by Woody and Richards.

Apart from the results of Woody and Richards, all reported measurements of the CBR temperature between 50 cm and 1 mm wavelength are consistent with a temperature of ~2.7 K and do not show evidence of significant departures from a blackbody spectrum. We are analyzing these data to derive limits on energy transfer between the matter and radiation fields in the early universe and to determine the extent to which various energy-releasing processes could have occurred. The initial results of our analysis are described in a paper by De Amici *et al.* (1985).

This experiment could not have been performed without the skilled help of many friends and colleagues. Our thanks to: J. Aymon, A. Benner, J. Costales, H. Dougherty, G. Epstein, V. Evans, J. Gates, J. Gibson, M. Griffith, B. Grossan, N. Gusack, L. Kelley, S. Levin, P. Lubin, and F. Mitschang. Special thanks to the staff and crew of the White Mountain Research Station for their ongoing assistance.

This work was supported by N.S.F. Grants No. PHY-8015694, AST-8302843, and AST-8406187, by the Department of Energy under Contract DE-AC03-76SF00098. and by C.N.R. Fellowships nos. 203.2.13 and 203.2.15.

APPENDIX A
COLD-LOAD ANTENNA TEMPERATURE

The antenna temperature of the cold load, $T_{A,\mathrm{Load}}$, is the sum of contributions from the cold Eccosorb target ($T_{A,\mathrm{Target}}$), from the aluminum-coated surface of the radiometric wall ($T_{A,\mathrm{Wall}}$), and from the windows ($T_{A,\mathrm{Windows}}$):

$$T_{A,\mathrm{Load}} = T_{A,\mathrm{Target}} + T_{A,\mathrm{Wall}} + T_{A,\mathrm{Windows}} . \qquad (A.1)$$

The temperature of the Eccosorb target is that of the boiling LHe in which it is immersed. Measurements of the target temperature and the ambient pressure within the load yield a physical temperature of 3.776 ± 0.004 K. From equation (1), the value of $T_{A,\mathrm{Target}}$ at 3.3 mm is therefore 2.020 ± 0.004 K.

The emissivity and temperature profile of the radiometric wall, weighted by the antenna gain pattern, determine $T_{A,\mathrm{Wall}}$. Measurements of the near-field gain pattern and the wall temperature, together with estimates of the wall emissivity, yield a 10 ± 10 mK value for $T_{A,\mathrm{Wall}}$.

Emission and reflection from the two windows at the top of the cold load both contribute to $T_{A,\mathrm{Windows}}$. Measurements indicate that each window emits 9.2 ± 2.3 mK into the antenna. The radiation reflected into the antenna by the windows comes partly from the cold load and partly from the antenna itself; the proportions vary depending on the distance from antenna to window. Tests indicate that depending upon its position, the upper window reflects up to 1.0×10^{-3} of the power broadcast by the antenna back into the antenna, whereas the lower window is far enough from the antenna so that reflection from its surface can be neglected. The noise power generated by the radiometer is equal to that of a blackbody at ~70 K, so reflected noise from the radiometer adds from 0 to 70 mK, or 35 ± 35 mK, to the observed antenna temperature of the upper window. The windows also reflect radiation from the coupling plates, bellows, and radiometric wall into the antenna. All of these have low temperatures, low emissivities, or both. The reflected contribution from these sources is less than 6.0 mK and can therefore be neglected. The quantity $T_{A,\mathrm{Windows}}$, the sum of the emitted and reflected temperature contributions from both windows, has a value of 53 ± 35 mK.

From equation (A.1), the value of $T_{A,\mathrm{Load}}$ is 2.083 ± 0.037 K.

APPENDIX B
ATMOSPHERIC MODEL

The radiometric sky temperature is the sum of the thermal emission from all levels of the atmosphere and the CBR antenna temperature (the only significant astronomical source at 3.3 mm), slightly reduced by atmospheric absorption. Since the antenna used to observe the sky has a gain pattern of finite width, the measured temperature is actually a gain-weighted average of the sky temperatures over a range of zenith angles.

The antenna temperature of the sky measured when the antenna axis points toward a zenith angle Z can be expressed mathematically as the integral

$$T_{\mathrm{Sky}}(Z) = \int_0^{2\pi} d\phi \int_0^{\pi} d\chi\, g(\chi,\phi)\cos(\chi) \left[T_{A,\mathrm{CBR}} e^{-\tau(\infty,\psi)} + \int_0^{\infty} T(s) e^{-\tau(s,\psi)} \kappa(s) f(s,\psi) ds \right] . \qquad (B.1)$$

In the equation above, s is the height above the ground. The angles ψ, χ, and ϕ are respectively the zenith angle of the integration element, the angular separation of the integration element from the antenna axis, and the rotation angle of the integration element around the antenna axis. The angles ψ, χ, ϕ, and Z are related by the equation

$$\cos(\psi) = \cos(Z)\cos(\chi) + \sin(Z)\sin(\chi)\cos(\phi).$$

The function $g(\chi, \phi)$ is the normalized antenna gain pattern in a direction (χ, ϕ) in antenna-centered coordinates. The geometrical factor $f(s, Z)$ is the derivative of column length with respect to height [$\sec(Z)$ in a planar-slab model]. In a spherical geometry, it can be approximated as

$$\begin{aligned} f(s, Z) &\approx \sec(Z) - (s/R_0)\sec(Z)\tan^2(Z) \\ &= f_1(Z) - (s/R_0) f_2(Z) \end{aligned} \tag{B.2}$$

where

$$\begin{aligned} f_1(Z) &= \sec(Z)\,, \\ f_2(Z) &= \sec(Z)\tan^2(Z)\,, \end{aligned}$$

and R_0, the earth's radius, is 6400 km. The quantity $T(s)$ is the ambient temperature in kelvins at height s, modeled as

$$\begin{aligned} T(s) &= 280 - 6.5s && s \leq 9 \text{ km} \\ T(s) &= 222 && 9 < s < 21 \text{ km} \\ T(s) &= 177 + 2.1s && s \geq 21 \text{ km.} \end{aligned}$$

The formula is based on a tabulation of the 1962 U. S. Standard Atmosphere (Cole *et al.* 1965) with minor adjustments for the ambient temperature at ground level. The absorption coefficient $\kappa(s)$ specifies the atmospheric absorption per unit path length at height s. The term $\tau(s, \psi)$ represents the atmospheric opacity at zenith angle ψ, measured from the ground to height s.

The value of $\kappa(s)$ is the sum of the absorption coefficients for pressure-broadened lines of oxygen and water vapor. One can show (Ulaby, Moore, and Fung 1981) that the coefficients for both molecular species scale with height s approximately as

$$\kappa \sim P(s)\rho(s)T(s)^{-2}\,,$$

$P(s)$ being the ambient pressure at s and $\rho(s)$ being the density of the molecular species. The pressure variation is nearly exponential with altitude, and has a 7.7 km scale height. The density variation is also approximately exponential: the density scale heights for water vapor and oxygen are 2.2 km and 9.5 km respectively (Ulaby, Moore, and Fung 1981).

Using these approximations, one can model $\kappa(s)$ as

$$\kappa(s) \approx \frac{\tau_0}{I_1(\infty, s_0)} \frac{e^{-s/s_0}}{T(s)^2}\,, \tag{B.3}$$

with the effective scale height s_0 between 1.7 km (for water vapor) and 4.2 km (for oxygen). The integral $I_1(s, s_0)$ is defined as

$$I_1(s, s_0) \equiv \int_0^s \frac{e^{-s/s_0}}{T(s)^2} ds\,.$$

The presence of $I_1(\infty, s_0)$ in the denominator of equation $(B.3)$ assures that the integral $\int_0^\infty \kappa(s)ds$ is equal to the zenith opacity τ_0.

The opacity $\tau(s, \psi)$ in equation $(B.1)$ is related to $\kappa(s)$ by the integral

$$\tau(s, \psi) = \int_0^s \kappa(s') f(s', \psi) ds'\,.$$

From equations $(B.2)$ and $(B.3)$, $\tau(s, \psi)$ can be approximated as

$$\tau(h, \psi) \approx \frac{\tau_0}{I_1(\infty, s_0)} [f_1(\psi) I_1(s, s_0) - f_2(\psi) I_2(s, s_0)]\,, \tag{B.4}$$

where $I_2(s, s_0)$ is defined by the equation

$$I_2(s, s_0) \equiv \int_0^s \frac{s e^{-s/s_0}}{R_0\, T(s)^2} ds \; .$$

Because the atmosphere is optically thin ($\tau_0 \sim 0.04$ at the observing site), the exponential terms in equation $(B.1)$ can be expanded as power series in τ:

$$T_{\rm Sky}(Z) \approx \int_0^{2\pi} d\phi \int_0^{\pi} d\chi\, g(\chi,\phi)\cos(\chi)\Big\{ T_{A,\rm CBR}\left[1 - \tau(\infty,\psi) + \frac{\tau(\infty,\psi)^2}{2} - \frac{\tau(\infty,\psi)^3}{6}\right] + \int_0^{\infty} T(s)\kappa(s) f(s,\psi)\left[1 - \tau(s,\psi) + \frac{\tau(s,\psi)^2}{2}\right] ds \Big\} \; .$$

If one substitutes equations $(B.2)$, $(B.3)$, and $(B.4)$ into the equation above, the result is

$$\begin{aligned} T_{\rm Sky}(Z) \approx T_{A,\rm CBR} &+ \tau_0 \Bigg[\int_0^{2\pi} d\phi \int_0^{\pi} d\chi\, g(\chi,\phi)\cos(\chi)\Big\{\Big[\int_0^{\infty} \frac{e^{-s/s_0}}{I_1(\infty,s_0)\,T(s)} ds - T_{A,\rm CBR}\Big] f_1(\psi) \\ &- \Big[\int_0^{\infty} \frac{e^{-s/s_0}}{I_1(\infty,s_0)\,T(s)} (s/R_0)\, ds - \frac{I_2(\infty,s_0)}{I_1(\infty,s_0)} T_{A,\rm CBR}\Big] f_2(\psi)\Big\}\Bigg] \\ &- \frac{\tau_0^2}{2}\Big\{\int_0^{2\pi} d\phi \int_0^{\pi} d\chi\, g(\chi,\phi)\cos(\chi)\Big[2\int_0^{\infty} \frac{e^{-s/s_0} I_1(s,s_0)}{I_1(\infty,s_0)^2\,T(s)}\, ds - T_{A,\rm CBR}\Big] f_1(\psi)^2\Big\} \\ &+ \frac{\tau_0^3}{6}\Big\{\int_0^{2\pi} d\phi \int_0^{\pi} d\chi\, g(\chi,\phi)\cos(\chi)\Big[3\int_0^{\infty} \frac{e^{-s/s_0} I_1(s,s_0)^2}{I_1(\infty,s_0)^3\,T(s)}\, ds - T_{A,\rm CBR}\Big] f_1(\psi)^3\Big\} \; . \end{aligned} \qquad (B.5)$$

The terms in the equation $(B.5)$ have been grouped according to their τ_0 dependence; terms of order $I_2{\tau_0}^2$, $I_2{\tau_0}^3$, and ${\tau_0}^4$ have been neglected. The integral expressions in equation $(B.5)$, calculated numerically from the atmospheric model and the antenna gain pattern, can be represented by three temperature terms Γ_1, Γ_2, and Γ_3. One can then rewrite equation $(B.5)$ in simpler form:

$$T_{\rm Sky}(Z) \approx T_{A,\rm CBR} + \tau_0\Gamma_1(Z) - \frac{{\tau_0}^2}{2}\Gamma_2(Z) + \frac{{\tau_0}^3}{6}\Gamma_3(Z) \; . \qquad (B.6)$$

In particular, $T_{A,\rm Atm}$ is given by the equation:

$$T_{A,\rm Atm} = T_{\rm Sky}(0) \approx \Gamma_1(0)\tau_0 - \Gamma_2(0)\frac{{\tau_0}^2}{2} + \Gamma_3(0)\frac{{\tau_0}^3}{6} \; . \qquad (B.7)$$

One can define the temperature difference $\Delta T_{\rm Sky}$ as

$$\Delta T_{\rm Sky} \equiv \frac{1}{2}[T_{\rm Sky}(Z_1) - T_{\rm Sky}(Z_2) + T_{\rm Sky}(Z_3) - T_{\rm Sky}(Z_4)] \qquad (B.8)$$

for values of $T_{\rm Sky}$ measured at zenith angles Z_1 through Z_4. This is the quantity expressed in equation (4). Analogously, the terms $\Delta\Gamma_n$ (n from 1 to 3) are defined by the equation:

$$\Delta\Gamma_n \equiv \frac{1}{2}[\Gamma_n(Z_1) - \Gamma_n(Z_2) + \Gamma_n(Z_3) - \Gamma_n(Z_4)] \; . \qquad (B.9)$$

The quantity ϵ is defined in § VI*d* as $\Delta T_{\rm Sky}/\Delta\Gamma_1$. From equations $(B.6)$, $(B.8)$, and $(B.9)$, it can thus be approximated:

$$\epsilon \approx \tau_0 - \frac{\Delta\Gamma_2}{\Delta\Gamma_1}\frac{{\tau_0}^2}{2} + \frac{\Delta\Gamma_3}{\Delta\Gamma_1}\frac{{\tau_0}^3}{6} \; . \qquad (B.7)$$

One can invert equation ($B.10$) to solve for τ_0 and substitute the resulting expression into equation ($B.7$) to yield an expression for $T_{A,\mathrm{Atm}}$ as a function of ϵ:

$$T_{A,\mathrm{Atm}} \approx \Gamma_1(0)\epsilon + \frac{1}{2}\left[\frac{\Delta\Gamma_2}{\Delta\Gamma_1}\Gamma_1(0) - \Gamma_2(0)\right]\epsilon^2 + \frac{1}{2}\left\{\frac{1}{3}\left[\Gamma_3(0) - \frac{\Delta\Gamma_3}{\Delta\Gamma_1}\Gamma_1(0)\right] + \left[\frac{\Delta\Gamma_2}{\Delta\Gamma_1}\Gamma_1(0) - \Gamma_2(0)\right]\frac{\Delta\Gamma_2}{\Delta\Gamma_1}\right\}\epsilon^3 \qquad (B.11)$$

to third order in ϵ. If one defines the temperature terms $T_{\mathrm{Atm},1}$ through $T_{\mathrm{Atm},3}$ as

$$T_{\mathrm{Atm},1} = \Gamma_1(0)\ ,$$
$$T_{\mathrm{Atm},2} = \frac{1}{2}\left[\frac{\Delta\Gamma_2}{\Delta\Gamma_1}\Gamma_1(0) - \Gamma_2(0)\right]\ ,$$

and

$$T_{\mathrm{Atm},3} = \frac{1}{2}\left\{\frac{1}{3}\left[\Gamma_3(0) - \frac{\Delta\Gamma_3}{\Delta\Gamma_1}\Gamma_1(0)\right] + \left[\frac{\Delta\Gamma_2}{\Delta\Gamma_1}\Gamma_1(0) - \Gamma_2(0)\right]\frac{\Delta\Gamma_2}{\Delta\Gamma_1}\right\}\ ,$$

equation ($B.11$) reduces to equation (4), the formula used to compute $T_{A,\mathrm{Atm}}$ from measurements of ΔT_{Sky}.

REFERENCES

Boynton, P. E., Stokes, R. A., and Wilkinson, D. T. 1968, *Phys. Rev. Letters,* **21,** 462.

Boynton, P. E., and Stokes, R. A. 1974, *Nature,* **247,** 528.

Cole, A., Court, A., and Kantor, A. 1965, in *Handbook of Geophysics and Space Environment,* ed. S. L. Valley (New York: McGraw-Hill).

Danese, L., and De Zotti, G. 1977, *Riv. Nuovo Cimento,* **7,** 277.

Danese, L., and De Zotti, G. 1978, *Astr. Ap.,* **68,** 157.

Danese, L., and De Zotti, G. 1980, *Astr. Ap.,* **84,** 364.

Danese, L., and De Zotti, G. 1982, *Astr. Ap.,* **107,** 39.

De Amici, G., Smoot, G. F., Friedman, S. D., and Witebsky, C. 1985, *Ap. J.,* **298,** 710.

De Amici, G., Witebsky, C., Smoot, G. F., and Friedman, S. D. 1984, *Phys. Rev. D,* **29,** 2673.

Ewing, M. S., Burke, B. F., and Staelin, D. H. 1967, *Phys. Rev. Letters,* **19,** 1251.

Friedman, S. D. 1984, Ph. D. thesis, University of California, Berkeley. UCLBL Report 17279.

Friedman, S. D., Smoot, G. F., De Amici, G., and Witebsky, C. 1984, *Phys. Rev. D,* **29,** 2677.

Jansen, M. A., Bednarczyk, S. M., Gulkis, S., Marlin, H., and Smoot, G. F. 1979, *IEEE Trans.,* **AP-27,** 551.

Kislyakov, A. G., Chernyshev, V. I., Lebskii, Yu. V., Mal'tsev, V. A., and Serov, N. V. 1971, *Astron. Zh.,* **48,** 39 (1971, *Sov. Astron.,* **15,** 29).

Lorrain, P., and Corson, D. R. 1970, *Electromagnetic Fields and Waves* (San Francisco: Freeman) § 12.5.

Mandolesi, N., Calzolari, P., Cortiglioni, S., Morigi, G., Danese, L., and De Zotti, G., 1986, *Ap. J.,* submitted.

Meyer, D. M., and Jura, M. 1985, *Ap. J.,* **297,** 119.

Millea, M. F., McColl, M., Pederson, R. J., and Vernon, F. L. 1971, *Phys. Rev. Letters,* **26,** 919.

Partridge, R. B., Cannon, J., Foster, R., Johnson, C., Rubinstein, E., and Rudolph, A. 1984, *Phys. Rev. D,* **29,** 2683.

Peebles, P. J. 1971, *Physical Cosmology* (Princeton: Princeton University Press).

Peterson, J. B., Richards, P. L., and Timusk, T. 1985, *Phys. Rev. Letters,* **55,** 332.

Sironi, G., and Bonelli, G., 1986, *Ap. J.,* submitted.

Smoot, G. *et al.* 1983, *Phys. Rev. Letters,* **51,** 1099.

Smoot, G. *et al.* 1985, *Ap. J. (Letters),* **291,** L23.

Stokes, R. A., Partridge, R. B., and Wilkinson, D. T. 1967, *Phys. Rev. Letters,* **19,** 1199.

Ulaby, F., Moore, R., and Fung, A. 1981, *Microwave Remote Sensing,* Vol. **1,** *Microwave Remote Sensing Fundamentals and Radiometry* (Reading: Addison-Wesley) (see eq. [5.20], [5.22], and [5.33] through [5.38] for the derivation of κ).

Weiss, R. 1980, *Ann. Rev. Astr. Ap.,* **18,** 489.

Welch, W. J., Keachie, S., Thornton, D. D., and Wrixon, G. 1967, *Phys. Rev. Letters,* **18,** 1068.

Wilkinson, D. T. 1967, *Phys. Rev. Letters,* **19,** 1195.

Witebsky, C. 1985, Ph. D. thesis, University of California, Berkeley. UCLBL Report 18746.

Woody, D. P., and Richards, P. L. 1979, *Phys. Rev. Letters,* **42,** 925.

Woody, D. P., and Richards, P. L. 1981, *Ap. J.,* **248,** 18.

CHRIS WITEBSKY, GEORGE SMOOT, and GIOVANNI DE AMICI: 50/232 Lawrence Berkeley Laboratory, University of California, Berkeley, CA 94720

SCOTT FRIEDMAN: CASS C-011, University of California at San Diego, La Jolla, CA 92093